INSTITUTE OF PHYSICS PUBLISHING JOURNAL OF PHYSICS: CONDENSED MATTER

J. Phys.: Condens. Matter **15** (2003) 4387–4395 PII: S0953-8984(03)61998-3

Non-local screened-exchange calculations for defects in semiconductors: vacancy in silicon

J Lento and R M Nieminen

Laboratory of Physics, Helsinki University of Technology, PO Box 1100, FIN-02015 HUT, Finland

E-mail: juha.lento@hut.fi

Received 10 April 2003
Published 13 June 2003
Online at stacks.iop.org/JPhysCM/15/4387

Abstract

The microscopic structure of a silicon vacancy is studied theoretically using first-principles supercell calculations. Both the standard Kohn–Sham local-density approximation (LDA) scheme and the generalized Kohn–Sham screened-exchange local-density approximation (sX-LDA) scheme are used. The latter approximation is expected to improve the description of electronic levels in the gap region substantially, while providing accurate total energies and bond lengths.

The present LDA calculations are in line with the earlier corresponding calculations of the silicon vacancy, predicting an inward relaxation of the nearest neighbours of the vacant site. The LDA calculations also predict the Jahn–Teller distortions and negative effective-U effects for charged vacancies, qualitatively in agreement with the experimental results and the Watkins model. In contrast to LDA results, the present sX-LDA calculations predict an *outward* relaxation and sp^2 type hybridization for the ions surrounding the vacancy. This somewhat surprising result is explained by the removal of the systematic overbinding associated with LDA.

1. Introduction

Density-functional theory (DFT) [1] provides a practical theoretical means to investigate complex many-body problems at the electronic structure level in many important areas of computational physics, chemistry and biology. The most successful and widely used realizations of the DFT are based on the standard Kohn–Sham (KS) scheme [2]. The use of auxiliary single-particle orbitals in the KS scheme for the description of kinetic energy yields a dramatic improvement in the calculated electronic structures of atoms, molecules and solids, compared to functionals where the kinetic energy is estimated from the electron density alone, as for example in the Thomas–Fermi approximation [3]. The many-particle interactions in the standard KS scheme are grouped into an exchange–correlation (xc)

functional. This unknown functional is usually approximated in an averaged fashion using the local-density approximation (LDA) or the generalized-gradient approximation (GGA). The success of these approximations has built up gradually, as experience has accumulated on their use in a wide variety of systems [3]. As an important extension, the generalized Kohn–Sham (GKS) scheme provides a theoretically solid framework in which to construct new improved realizations of the density-functional theory [4, 5].

Local and quasi-local functionals of the density, such as LDA and GGA, cannot describe the discontinuity of the xc potential with respect to particle number, which is considered to be one of the reasons for a major shortcoming of the LDA, the band-gap underestimation in semiconductors and insulators [6]. A qualitatively opposite problem is encountered with the Hartree–Fock method, which is known to considerably overestimate the band gaps. Moreover, its application in metallic systems leads to well known problems, such as a vanishing density of states at the Fermi level. Intuitively, a hybrid method 'interpolating' between the two seems to be a potentially effective approach [5].

In a similar spirit as with the use of auxiliary single-particle orbitals in the evaluation of kinetic energy in the standard KS scheme, the auxiliary single-particle orbitals can be used to also evaluate other parts of the total energy functional in the GKS scheme. In the screened-exchange LDA (sX-LDA) realization of the GKS scheme the single-particle orbitals are used to construct a non-local exchange operator improving the description of the exchange interaction compared to LDA. The many-body correlations and screening missing from the pure Hartree–Fock method are treated in a form of model screening and LDA correlation [4].

The previous applications of the sX-LDA method have concentrated on the possibility of using the GKS eigenvalues in the description of the band structures of crystals and surfaces [4, 7–9]. As part of the discontinuity in the xc potential is incorporated in the GKS eigenvalues, the comparison of the eigenvalues with the experiment is more favourable. In general, the agreement with experiment has been shown to be comparable to the predictions from perturbation theory using Hedin's GW approximation [10]. One of the particular cases where qualitative improvement has been reported is germanium, where LDA yields a zero energy gap, but sX-LDA correctly regains a finite value. However, one has to note that these band structure calculations [4, 7] are done using the experimental lattice parameter $a_{\mathrm{Ge}}^{exp} = 5.66$ Å, which practically coincides with the theoretical equilibrium lattice parameter of sX-LDA, but deviates slightly from the LDA value $a_{\mathrm{Ge}}^{LDA} = 5.56$ Å. The consistent use of the theoretical equilibrium lattice constant and the removal of the spurious external applied pressure effects on the band positions in the LDA calculations renders the difference less dramatic [11]. As sX-LDA provides a total energy functional equivalent to LDA, it can also be used to evaluate structural properties. Previously it has been shown to reduce the overbinding associated with LDA, yielding equilibrium lattice parameters close to experimental values [4].

The silicon vacancy can be considered as the simplest example of a point defect in a semiconductor. Despite its apparent simplicity, the silicon mono-vacancy is a highly nontrivial test system for computational methods beyond perturbation approaches due to the complicated interaction between the electronic structure and ionic relaxations. There exists a wealth of experimental data, model Hamiltonians and detailed LDA/GGA calculations of the vacancy [12–15]. The consensus at the moment is that the vacancy is qualitatively described by the Watkins linear combination of atomic orbitals (LCAO) model [12]. In this model, four dangling bond orbitals directed towards the centre of the vacancy are formed. The symmeric linear combination a_1 accommodating two electrons is an s-like state, and it lies in energy within the valence band. In a doubly positive charge state the p-type t_2-triplet level is empty and the vacancy remains in the perfect lattice T_d-point symmetry. When electrons are added to the defect, the degeneracy of the t_2 level is lifted and the symmetry of the defect is reduced first

to D_{2d} for singly positive (V_{Si}^{1+}) and neutral (V_{Si}^{0}) charge states and then to C_{2v} for the negative charge states (V_{Si}^{1-}) and (V_{Si}^{2-}) resulting in a lower total energy compared to T_d symmetric configurations. In addition to this Jahn–Teller effect, the silicon vacancy also exhibits the negative effective-U effect, in which the effects of the symmetry lowering lattice relaxation from T_d to D_{2d} more than compensate for the Coulomb repulsion between electrons in the localized defect orbitals. The capture of a single electron to the doubly positive charge state is immediately followed by a capture of another electron, and the singly positive charge state is not energetically stable for any value of the electron chemical potential.

The experimental evidence supporting the Jahn–Teller distortions and the negative effective-U effect in the Watkins model is strong [12]. On the other hand, the determination of the magnitude, and even the direction, of the breathing mode relaxation from experiments relies on rather indirect methods. According to theoretical estimates, the positron lifetime (PLT) for the silicon vacancy depends strongly on the open volume of the vacancy [16]. Assuming that the form of the electron–positron correlation remains the same in different charge states of the vacancy, this directly relates the changes in the positron lifetime to the changes in the open volume of the vacancy in different charge states. The PLT measurements of the vacancy–phosphorus pair, thus interpreted with the help of theoretical results, imply that the breathing mode relaxation of the negative charge state $(V_{Si}–P)^{1-}$ is almost negligible and the neutral charge state $(V_{Si}–P)^{0}$ relaxes ∼5% outwards [17]. The outward relaxations estimated from the deep-level transient spectroscopy (DLTS) measurements of a vacancy–phosphorus pair under hydrostatic pressure are ∼3 and ∼6% for $(V_{Si}–P)^{1-}$ and $(V_{Si}–P)^{0}$, respectively [18].

The previous systematic theoretical study [13] has demonstrated that the Born–Oppenheimer surface for the vacancy is relatively flat and possesses several nearly degenerate local minima with different local symmetries, which makes the silicon vacancy particularly sensitive to the supercell size and different numerical approximations. The LDA calculations presented in this paper are in line with previous LDA and GGA calculations [13, 14], with an accompanying *inward* breathing-mode relaxation of the nearest-neighbour (NN) ions of the vacant site in all charge states.

In contrast to the LDA results, the present sX-LDA calculations indicate an *outward* breathing-mode relaxation of the vacancy in all charge states. The outward relaxation and the sp^2 type bonding of the NN ions of the vacant site to the rest of the host lattice was already proposed based on the early Green function calculations [19] and presents an alternative to inward relaxation predicted by the LDA/GGA.

The main purpose of this paper is to report on the feasibility of the self-consistent sX-LDA calculations for large supercells required for accurate description of point defects in semiconductors and insulators. Such calculations, even without the non-local exchange potential, are computationally very demanding, as they require the simultaneous consideration of finite-size (supercell) effects, computational convergence and xc approximations. We use well-tested plane-wave pseudopotential methods for the classic test case, the silicon vacancy.

2. The LDA calculations

We have performed first-principles DFT calculations for the silicon vacancy using 32 and 256 atomic-sites body-centred cubic (BCC) supercells. The core electrons are described using norm-conserving pseudopotentials [20] generated within the LDA and without non-linear core corrections [21]. The valence electron orbitals are described in a plane-wave basis with a cut-off energy of 15 Ryd. The LDA correlation energy is given by the parametrized [22] Ceperley and Alder [23] quantum Monte Carlo data. The first Brillouin zone (BZ) is sampled using

Table 1. Distances between the NN ions of a vacant site in 32- and 256-atom supercells calculated with LDA in different charge states q. The ideal theoretical NN distance is 3.81 Å for LDA. The eighth column, $\Delta\Omega = 100(V - V_0)/V_0$, is the change in the vacancy volume relative to the corresponding volume in a perfect Si crystal. The local point-group symmetry based on the NN ion positions is shown in the last column.

32-atomic site BCC supercell, LDA					
q	(1)–(2)	(3)–(4)	(5)–(6)	$\Delta\Omega$	Symmetry
(2+)	3.970	3.970	3.970	12.9	T_d
(1+)	3.831	3.831	3.709	−2.0	D_{2d}
(0)	3.608	3.608	3.084	−30.2	D_{2d}
(1−)	3.592	3.504	3.222	−28.0	D_2
(2−)	3.531	3.269	3.269	−32.9	D_{2d}
256-atomic site BCC supercell, LDA					
(2+)	3.684	3.685	3.685	−9.7	T_d
(1+)	3.475	3.475	3.155	−32.3	D_{2d}
(0)	3.490	3.490	2.950	−40.8	D_{2d}
(1−)	3.380	3.259	2.956	−42.8	D_2
(2−)	3.312	2.998	2.998	−47.6	D_{2d}

the (1/4,1/4,1/4) point [24]. The 256-atom BCC supercell allows ionic relaxations within LDA and provides the most accurate LDA calculations for the vacancy reported. A uniform compensating charge is used to render the supercell neutral in the calculation of charged states and the error associated with this approximation is estimated using a Madelung-type correction [25]. The theoretical equilibrium lattice parameter $a_{LDA} = 5.39$ Å was obtained using a 2-atom face-centred unit cell with eight irreducible k points in the first BZ [26].

The LDA vacancy geometries calculated using the 32-atom supercell agree qualitatively with the 256-atom supercell results (see table 1) and are in line with previous calculations [13, 14]. The optimal k-point sampling and the use of a BCC supercell minimize the errors caused by the defect–defect interactions, and the 32-atom results compare surprisingly well with the ones acquired with larger supercells and multiple k-point sampling schemes [13]. Notably, the local symmetries obtained with the 32-atom supercell coincide with the 256-atom results. The breathing mode relaxation is inwards in all charge states, except for the doubly positive vacancy, and increases as more electrons are bound to the vacancy. The inward relaxation of the doubly positive vacancy is only obtained with supercells larger than roughly 200 atoms [13]. The general trend of stronger binding with LDA than GGA is seen in the comparison of the lattice relaxation volumes for the neutral vacancy in a 256-atom supercell. The relaxation volumes obtained using LDA and GGA are $\Delta\Omega(\mathrm{LDA}) = -41\%$ and $\Delta\Omega(\mathrm{GGA}) = -27\%$ [14], respectively.

The present LDA calculations agree with the symmetry lowering lattice relaxation patterns in the Watkins LCAO model [12] for positive and neutral charge states. In the Watkins model the third and fourth localized gap electrons, corresponding to the charge states V_{Si}^{1-} and V_{Si}^{2-}, form an anti-bonding orbital between two ions neighbouring the vacancy. This would indicate that one of the shorter bonds (5)–(6) in table 1 expands slightly compared to the other. The calculated geometries show the formation of four short bonds, disagreeing with the LCAO model. The discrepancy with the LCAO model can be associated with the large lattice relaxations and the mixing of the dangling bond orbitals with conduction band states, as the defect-level dispersion in the 216-atom supercell is estimated to be still of the order of 0.2 eV [13].

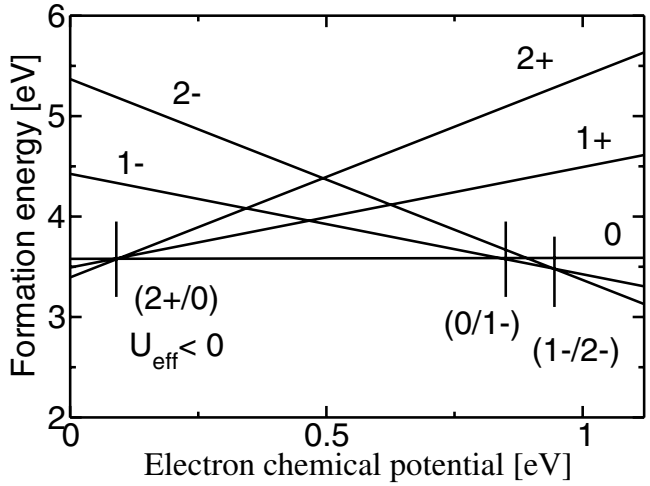

Figure 1. Formation energy of the vacancy in charge states from 2+ to 2− as a function of the electron chemical potential μ_e. The positions of the ionization levels are shown as vertical full lines.

The formation energies and ionization levels are calculated from the LDA total energies of the 256-atom supercells. The formation energy of the defect $E_V^{(q)}$ in charge state q as a function of the electron chemical potential μ_e measured from the top of the valence band ϵ_v is determined from

$$E_V^{(q)} = E_{N-1}^{(q)} - \frac{N-1}{N} E_N + q(\mu_e + \epsilon_v), \tag{1}$$

where $E_{N-1}^{(q)}$ is the total energy of the supercell containing the defect, N is the number of atoms in the supercell and E_N is the total energy of a N-atom perfect silicon crystal supercell [27]. The total energies of the charged supercells with a uniform compensating background charge are corrected using a Madelung-type first-order correction, which for the 256-atom BCC supercell is $\Delta E = 0.1q^2$ eV [25], and which is taken into account in figure 1. The ionization levels are defined as the values of the electron chemical potential μ_e in which the thermodynamically most stable charge state changes, indicated as short vertical lines in figure 1.

The formation energy calculated for the neutral vacancy in the present work using a 256-atom supercell and the LDA is $E_V^0(\text{LDA}, 256) = 3.6$ eV. This can be compared with an earlier LDA result using a 216-atomic-sites simple-cubic supercell, giving $E_V^0(\text{LDA}, 216) = 3.3$ eV [13] and $E_V^0(\text{LDA}, 216) = 3.17$ eV obtained using a 256-atom supercell and GGA [14]. The differences in the absolute values of the calculated formation energies can be assigned to several numerical factors differing in the calculations, the pseudopotentials used and xc descriptions for example, and thus suit general estimation of the accuracy of these state-of-the-art methods.

The electron chemical potential μ_e is, in principle, given relative to the valence band maximum ϵ_v occurring at the Γ point. The positions of the ionization levels depend linearly on the choice of ϵ_v. As the first BZ in our supercell calculation is sampled using the (1/4,1/4,1/4) point only, we use the value $\epsilon_v = 3.36$ eV of the highest valence KS eigenvalue of the corresponding perfect crystal supercell at that point. This choice also corresponds to the simple total energy difference of the neutral and singly positive perfect lattice supercell, explicitly describing the removal of an electron from the reservoir.

The ionization levels in figure 1 calculated using the 256-atom supercell agree with the experimental results [12] and are in line with previous calculations [13]. The ionization levels for the 32-atom supercell are not shown, as the small supercell size effectively restricts the necessary lattice relaxations and all the ionization levels are far too high in energy. The trend of overestimated ionization level positions in small supercells can be seen in a previous systematic study [13]. Also, the magnitude of the approximate $\Delta E = 0.2q^2$ eV correction for the compensating background charge in the 32-atom supercell is relatively large compared to the band gap, and the average potential correction [13] for the 32-atom supercell is $\sim$0.2 eV, i.e. significant compared to the almost negligible value of $\sim$0.03 eV for the 256-atom supercell.

3. The sX-LDA calculations

The GKS method offers a possibility to split up the total energy in such a way that the variational single-particle equations contain the screened-exchange potential. The GKS equations within the sX-LDA [4] are

$$[-\tfrac{1}{2}\nabla^2 + v_{eff}(r)]\phi_i(r) - \int \mathrm{d}r' v_x^{sx,NL}(r,r')\phi_i(r') = \epsilon_i\phi_i(r), \tag{2}$$

$$v_x^{sx,NL}(r,r') = -\sum_{j=1}^{N} \frac{\phi_j(r)\mathrm{e}^{-k_{TF}|r-r'|}\phi_j^*(r')}{|r-r'|}, \tag{3}$$

where the effective local potential is modified so that the functional remains exact at the limit of a homogeneous electron gas $v_{eff}(r) = v_{eff}^{LDA}(r) - v_x^{sx}(r)$ [4]. The Thomas–Fermi screening was chosen with a wavevector $k_{TF} = 2.1$ Å^{-1} corresponding to the average bulk valence-electron density in silicon. The choice of the model dielectric screening function is not unique, and other models have been presented [4, 5].

The non-local term of the sX-LDA functional introduces an increase in computational cost comparable to the Hartree–Fock method. The numerical efficiency of the LDA implemented in the plane-wave basis is explained by two factors. First, the kinetic energy operator and the effective local potential are diagonal in reciprocal and real-space representations, respectively. Second, the transformation from the real space to the reciprocal space and the evaluation of the convolution-type products in the Coulomb integrals are effectively performed using the fast Fourier transform (FFT). The FFT can also be used to speed up the evaluation of the convolution-type products in the non-local screened-exchange operator. Even with the use of FFT in the evaluation of the non-local integrals, one still faces extra double summations over the electronic states and k points in the evaluation of the total energy. The use of the inherent crystal symmetries with 'special k-point sets' in the evaluation of the BZ integrals becomes more complicated for the non-local term. With the double summation it increases the computational work, especially when calculating metallic systems, where the description of the Fermi surface requires a large number of k points. We also note that the matrix $\langle i|v_x^{sx,NL}|j\rangle$ is usually dense, so the double summation over the states cannot be restricted to some subsets of the states.

We use the Car–Parrinello-type Williams–Soler [28] iteration scheme for the electronic degrees of freedom, in which the effective potential is updated for each eigenstate iteration step. This differs from the conjugate-gradient density-mixing-type schemes where the KS states are solved for a fixed effective potential, and after the solution is found the effective potential is updated to reach self-consistency. With the current implementation of the sX-LDA we are able to perform roughly one electronic iteration (one evaluation of the non-local term)

Table 2. The total energies for various fixed ionic configurations for a neutral vacancy using LDA and sX-LDA with $a_{sx} = 5.44$ Å. The distance of the first-neighbours shell from the vacant site d_1 is given in ångströms. The total energies are given in electronvolts, relative to the ideal structures calculated for both functionals separately.

Ion configuration	d_1	E_{tot}^{LDA}	E_{tot}^{sX}
Ideal	2.356	0	0
Relaxed 256 LDA	2.095	−0.415	1.2
Embedded 32 sX-LDA	2.890	1.215	−0.5

in four CPU hours for a 256-atom supercell, compared to 12 iterations per CPU hour with LDA, when using eight Power4 processors in an IBM pSeries 690 server.

The geometries optimized using the sX-LDA functional and the equilibrium sX-LDA lattice parameter $a_{sX} = 5.44$ Å in the 32-atom supercell differ qualitatively from the ones obtained using LDA. The NN ions relax strongly *outwards* in all charge states. The outward relaxation of the first shell ions increases monotonically as the charge state changes from V_{Si}^{2+} to V_{Si}^{2-}, with the distances from the vacant site increasing from 20 to 36%. The bonding between the first- and second-neighbour shell ions resembles the more planar sp^2 type bonding than the tetrahedral sp^3 bonding. The lengths of the sp^2 bonds remain roughly the same, 2.3 Å, in all charge states, with corresponding angles in sp^2 varying from 118° to 120°.

The 32-atom supercell is clearly too small to relieve the elastic stress of the strong outward relaxation. To gain more confidence on the outward relaxation result, we have also performed calculations with a 256-atom BCC supercell and the sX-LDA lattice parameter. Since the number of evaluations of the non-local term (equation (3)) required for complete ionic relaxation is of the order of thousands, and we are limited to tens of iterations in the sX-LDA calculation, we can only compare the total energies and forces on ions for fixed ionic configurations. The KS orbitals in all cases are first iterated using LDA until a self-consistent electronic ground state is found. The functional is then switched to sX-LDA and a further 30 electronic iteration steps are run starting from the LDA KS orbitals.

The results for a 256-atom BCC supercell presented in table 2 and figure 2 support the breathing-mode relaxation patterns already shown in the fully relaxed 32-atom supercell calculations. The fully relaxed LDA minimum energy structure (*relaxed 256 LDA*), even with the sX-LDA lattice parameter, shows inward relaxation very similar to the calculation using the equilibrium LDA lattice parameter. The total energies clearly show that the optimal LDA ionic structure is *not* the minimum energy structure for sX-LDA. Even unrelaxed ideal positions of the crystal (*ideal*) give a sX-LDA total energy that is lower than the total energy of the inward-relaxed structure predicted by LDA. The average forces on ion shells surrounding the vacancy in *ideal* positions are shown in table 2. The difference between the LDA and sX-LDA forces in the first-neighbour shell is clear, the LDA favouring inward relaxation and the sX-LDA favouring outward relaxation. The forces on further shells are almost identical.

The outward stresses (in the sX-LDA) in different charge states for the *ideal* structure agree with the experimental results [17, 18] that in electron emission $V_{Si}^{q} \rightarrow V_{Si}^{q+1}$ the volume of the vacancy increases. The outward force on the first ion shell increases roughly 40% in charge state 2+ and decreases roughly the same amount in charge state 2− compared to the forces for a neutral charge state.

The lowest sX-LDA total energy is achieved for the ionic structure in which the fully relaxed 32-atom supercell is embedded in an otherwise ideal 256-atom supercell (*embedded 32 sX-LDA*). In the *embedded 32 sX-LDA* calculation the residual forces on first shell ions are negligible compared to forces in the *ideal* calculation, −0.01 and 0.5 au, respectively,

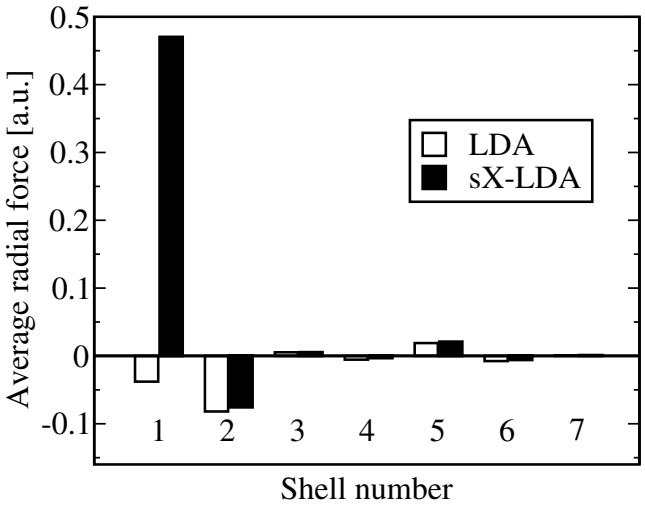

Figure 2. The average breathing-mode forces on ions in ideal positions for a neutral vacancy with the lattice parameter $a_{sx} = 5.44$ Å. The negative sign corresponds to inward stress.

suggesting that the immediate neighbourhood of the vacancy is described more accurately in the *embedded 32 sX-LDA* configuration. In addition, the residual forces on other ions in the embedded supercell are slightly larger than in other calculations, implying a larger potential for reduction in the total energy when the lattice is allowed to relax, adding still more support to the outward relaxation result.

We explain the outward relaxation within the sX-LDA with the removal of the systematic LDA overbinding [3]. The outward lattice relaxation is not a mere consequence of the increased lattice parameter, as the LDA calculations with the sX-LDA lattice parameter retain the inward relaxation, as do the GGA calculations with $a_{GGA} = 5.43$ Å for a neutral vacancy [14].

4. Summary

We have demonstrated that the sX-LDA method is a viable alternative to the LDA and GGA realizations of the local-density theory, not only in the calculation of the band structures, but also in the calculation of the fully self-consistent solutions to the electronic and ionic structures of point defects in semiconductors. With the most accurate LDA calculations of the silicon vacancy to date, we demonstrate that the dependence of the results on the numerical approximations, especially the supercell size, is reduced to an acceptable level. The present implementation of the sX-LDA allows us to perform full ionic relaxations of the modest size 32-atom supercells and self-consistent electronic structure calculations of large 256-atom supercells with fixed ionic positions.

The present calculations show definite qualitative differences between the LDA and sX-LDA descriptions of the silicon vacancy. The LDA results in an inward relaxation and Jahn–Teller distortions of the NNs of the vacant site, in agreement with the Watkins model and the experimental results. The sX-LDA leads to an outward relaxation of the vacancy, with the sp^2 type bonding of the NNs of the vacancy to the rest of the lattice. Complete ionic relaxation calculations in the 256-atom supercell for silicon vacancy are needed before decisive comparison to experiments can be made concerning sX-sLDA.

Acknowledgments

This research has been supported by the Academy of Finland through its Centre of Excellence Programme (2000–2005). JL would also like to thank Professor M Puska for invaluable discussions, the Center for Scientific Computing (CSC) for generous computational resources and the Väisälä, Wihuri and Nokia Foundations for financial support.

References

[1] Hohenberg P and Kohn W 1964 *Phys. Rev.* B **136** 864
[2] Kohn W and Sham L J 1965 *Phys. Rev.* A **140** 1133
[3] Jones R O and Gunnarsson O 1989 *Rev. Mod. Phys.* **61** 689
[4] Seidl A, Görling A, Vogl P, Majewski J A and Levy M 1996 *Phys. Rev.* B **53** 3764
[5] Engel G E 1997 *Phys. Rev. Lett.* **78** 3515
[6] Perdew J P and Levy M 1983 *Phys. Rev. Lett.* **51** 1884
Sham L J and Schlüter M 1983 *Phys. Rev. Lett.* **51** 1888
[7] Bylander B M and Kleinman L 1990 *Phys. Rev.* B **41** 7868
[8] Asahi R, Mannstadt W and Freeman A J 2000 *Phys. Rev.* B **62** 2552
[9] Picozzi S, Continenza A, Asahi R, Mannstadt M, Freeman A J, Wolf W, Wimmer E and Geller C B 2000 *Phys. Rev.* B **61** 4677
[10] Hedin L 1965 *Phys. Rev.* A **139** 796
[11] Fiorentini V 1992 *Phys. Rev.* B **46** 2086
[12] Watkins G D 1986 *Deep Centers in Semiconductors* ed S T Pantelides (New York: Gordon and Breach) p 147
[13] Puska M J, Pöykkö S, Pesola M and Nieminen R M 1998 *Phys. Rev.* B **58** 1318
[14] Probert M I J and Payne M C 2003 *Phys. Rev.* B **67** 075204
[15] Baraff G A, Kane E O and Schlüter M 1980 *Phys. Rev.* B **21** 3563
[16] Puska M J and Corbel C 1988 *Phys. Rev.* B **38** 9874
[17] Mäkinen J, Hautojärvi P and Corbel C 1992 *J. Phys.: Condens. Matter* **4** 5137
[18] Samara G A 1988 *Phys. Rev.* B **37** 8523
Samara G A 1989 *Phys. Rev.* B **39** 12764
[19] Scheffler M, Vigneron J P and Bachelet G B 1985 *Phys. Rev.* B **31** 6541
[20] Troullier N and Martins J L 1991 *Phys. Rev.* B **43** 1993
[21] Louie S G, Froyen S and Cohen M L 1982 *Phys. Rev.* B **26** 1738
[22] Perdew J P, Burke K and Wang Y 1996 *Phys. Rev.* B **54** 16533
Perdew J P, Jackson K A, Pederson M R, Singh D J and Fiolhais C 1992 *Phys. Rev.* B **46** 6671
[23] Ceperley D M and Alder B J 1980 *Phys. Rev. Lett.* **45** 566
[24] Makov G, Shah R and Payne M C 1996 *Phys. Rev.* B **53** 15513
[25] Lento J, Mozos J-L and Nieminen R M 2002 *J. Phys.: Condens. Matter* **14** 2637
[26] Moreno J and Soler J M 1992 *Phys. Rev.* B **45** 13891
[27] Zhang S B and Northrup J E 1991 *Phys. Rev. Lett.* **67** 2339
[28] Tassone F, Mauri F and Car R 1994 *Phys. Rev.* B **50** 10561
Williams A and Soler J 1986 *Bull. Am. Phys. Soc.* **32** 562